Available online at www.sciencedirect.com
ScienceDirect
Trans. Nonferrous Met. Soc. China 30(2020) 1148−1156
Transactions of Nonferrous Metals Society of China
www.tnmsc.cn

Effect of Cu element on morphology of TiB_2 particles in TiB_2/Al−Cu composites

Jing SUN[1,2], Xu-qin WANG[1], Yan CHEN[1], Fei WANG[1], Hao-wei WANG[2]

1. Shanghai Aerospace Equipment Manufacturer Limited Company, Shanghai 200245, China;
2. State Key Laboratory of Metal Matrix Composites, Shanghai Jiao Tong University, Shanghai 200240, China

Received 6 August 2019; accepted 7 April 2020

Abstract: In order to explore the influence of Cu element on the morphology evolution of the in-situ TiB_2 particles, the 10 wt.% TiB_2 reinforced Al−5wt.%Cu based composite was prepared by mixed salt casting. The morphology characterization and transformation of TiB_2 reinforcements caused by Cu element were investigated by multi-scale microstructure characterization and statistics techniques. In the case of controlled casting, 5 wt.% Cu addition was found to transform the TiB_2 particle morphology from hexagonal plate with sharp edges and corners to hexagonal or tetragonal prism with chamfered edges and corners with the distinguishing growth steps both on the top surface and the side surface. The TiB_2 growth in Al−Cu matrix followed the rules: nano-scaled spherical nuclei—polyhedron grains—chamfered hexagonal particles—hexagonal plates—chamfered particles with obvious growth steps. The adsorption energy of Cu on different crystal surfaces of TiB_2 was caculated to reveal the influence mechanism and the results indicated that Cu was preferentially adsorbed on the $(10\bar{1}1)_{TiB_2}$ crystal planes, devoting to the small aspect ratio of TiB_2.

Key words: shape control; preferential adsorption; TiB_2 morphology; 2D-nucleation; growth step

1 Introduction

Aluminum and aluminum alloys are widely used in the aeronautical and automobile industries due to their low density, appropriate mechanical properties and high processability, whereas the limited strength of monotonous alloy restricts the further application prospects. A wealth of research verified the Al-based composite with the reinforcement of discontinuous ceramic particles, including TiC [1], SiC [2,3], Al_2O_3 [4,5] and so on, possessed dramatically enhanced strength and plasticity. Generally, according to the source of the reinforcement, the method of composite fabrication can be classified into ex-situ and in-situ. Compared to the conventional ex-situ composites, one of the prominent advantages of the in-situ metal matrix composites was the finer reinforcing particles distributing more uniformly in the matrix [6,7].

TiB_2 was usually used to reinforce composite materials [8−10]. Therefore, the size distribution, morphology, texture and the surface energy of TiB_2 seriously influenced the composite properties. WU et al [11] studied the influence of reinforced-TiB_2 size distribution on the microstructure and mechanical properties of the composites, suggesting that the grain size of TiB_2 dominantly influenced the fracture mode. With the increase of the TiB_2 size, the dominant fracture mode of the composites transformed from trans-granular fracture to inter-granular fracture. Moreover, it was worthy noticing that the in-situ TiB_2 exhibited distinguishing morphologies in different matrices. ZHANG et al [12] proposed that TiB_2 particles synthesized by laser surface alloying in AA6061

Foundation item: Project (2017YFB110400) supported by the National Key Research and Development Program of China
Corresponding author: Jing SUN; Tel: +86-21-24187153; Fax: +86-21-64300107; E-mail: 15216615475@163.com
DOI: 10.1016/S1003-6326(20)65285-2

matrix mainly exhibited hexagonal plate-like morphology and mainly distributed at high angle grain boundaries. QI et al [13] explored the fabrication of TiB_2 reinforced $(AlCrFeMnV)_{90}Bi_{10}$ alloy composite by spark plasma sintering and it was observed that TiB_2 exhibited irregularly blocky morphology. XIA et al [14] synthesized TiB_2/Cu composite by the in-situ reaction of Cu−Ti−B system, where the particles appeared as cubic sphere and the size was distributed in the range of 50−200 nm. ZOU et al [15] suggested that under the influence of La, the in-situ TiB_2 particles in TiB_2/Cu composite exhibited more uniform distribution and finer size, resulting in improved mechanical properties. Additionally, immense amount of researches about mechanical properties development and processing technology of TiB_2/Al composites were conducted recently [10,16−19]. In summary, plenty of work focused on the TiB_2 reinforced composites and the influence of reinforcement morphology on the material properties. However, limited attention has been paid to the crystal growth and morphology control mechanism of in-situ TiB_2 particles in the composite melt system.

Multiple researches indicated that the morphology and size of in-situ ceramic reinforcement could be significantly influenced by addition of alloying element. Alloying elements may change the particle size and morphology by preferentially adsorbing on some crystalline phases to inhabit the continuous growth, similar to the function of chemical surfactants. GAO et al [20] prepared the sphere, hexapod, hexagonal disk, nanocrystalline and nanoporous structure ZnO crystals merely by varying the concentration of F^- ions and the sintering temperature. They suggested that surfactants possessed remarkable ability to control crystal growth and directed it in shape and size controlled manner. BISWAS et al [21] indicated that TiO_2 nanorods could be synthesized using an anionic surfactant template. Therefore, it can be safely concluded that the desired morphologies can be achieved by controlling the preferential adsorption architecture as well as the self-assembly behavior. Hence, it is necessary to understand the nucleation and growth kinetics, including the microstructure evolution of TiB_2 crystals and the influence mechanism of different alloy elements.

However, limited attention has been paid to the crystal growth and morphology evolution involving in-situ TiB_2 particles in the composite melt system. In the present work, the morphology transformation of TiB_2 particles in TiB_2/Al matrix under the influence of Cu element was researched. Moreover, the growth mode of TiB_2 particles in Al−Cu matrix was illustrated both in schematic diagram and practical experiment results. Additionally, the current research provided a potentially convenient and feasible approach to control the morphologies of the in-situ TiB_2 reinforcement in Al matrix.

2 Experimental

The sample used was prepared from a commercially pure aluminum (CPAl) with the content of 5 wt.% Cu, and TiB_2 particles were formed by reactions of mixed salts (K_2TiF_6 and KBF_4). The metal ingot was melted in metal die which was placed in the resistance furnace and heated to about 750 °C. Then the mixed salts were added in a proper proportion and the melt was preserved at 850 °C for 1 h. The content of the generated TiB_2 was 10 wt.%. The temperature of the melt containing the in-situ TiB_2 particles was reduced to 750 °C and held for about 0.5 h before pouring into a preheated steel mold.

Metallographic samples were prepared from a piece of the solidified material, about *d*30 mm × 10 mm from the center of the cast ingot by mechanical grinding and polishing, followed by etching in a 0.5 vol.% HF aqueous solution for 3−4 min. The microstructure of the TiB_2/Al−Cu composite was examined using a scanning electric microscope (Nova Nano SEM). Statistical analysis on the size and shape factor of the TiB_2 particles was carried out using computer image processing facility.

3 Results and discussion

Under the influence of Cu, the typical morphology of TiB_2 crystals was shown in Fig. 1. In Fig. 1(a), TiB_2 exhibited typical hexagonal morphology with chamfered planes replacing the sharp corners and edges. Based on the characterization in the previous work [22], it could be concluded that the crystal surface was bound by the close-packed surface (0001), $(10\bar{1}0)$ and the

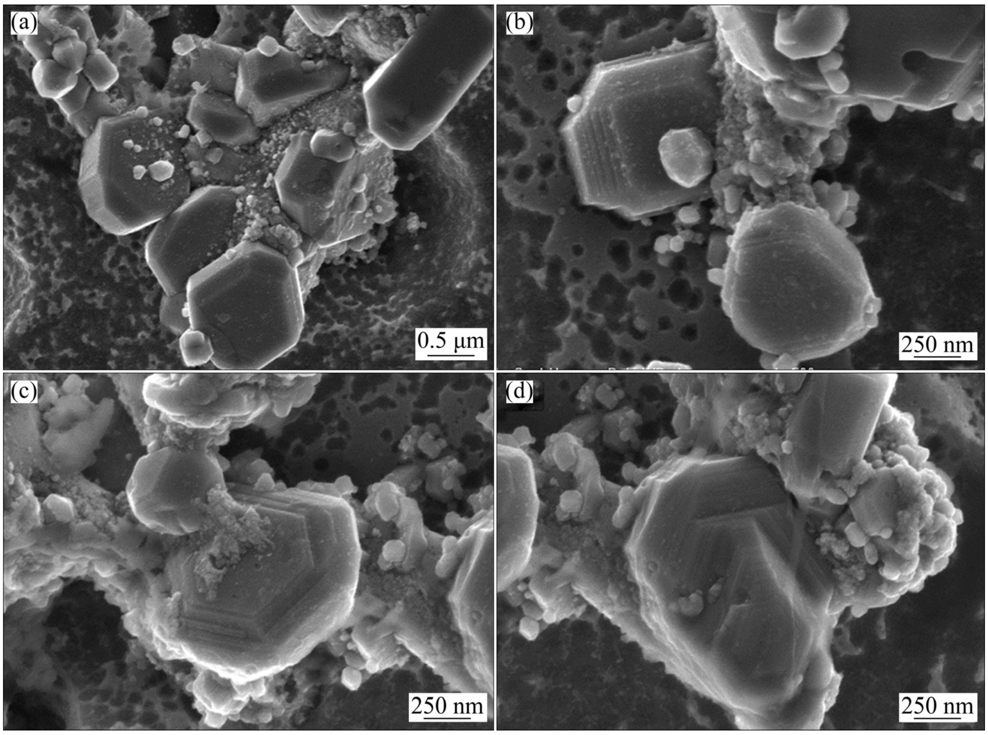

Fig. 1 Morphologies of TiB_2 particles in Al−5Cu matrix: (a) Chamfered hexagonal TiB_2; (b) Chamfered tetragonal TiB_2; (c) Growth step on top surface; (d) Obvious bulge on top surface

chamfered planes were established as $(10\bar{1}1)$ on the basic chamfered surface, $(11\bar{2}0)$ on the side chamfered surface and $(1\bar{2}1\bar{3})$ at the chamfered corner. Figure 1(b) showed a tetragonal TiB_2 particle exposed a nearly close-packed plane $(11\bar{2}0)$ and the close packed basic plane (0001) based on the HR-TEM revelation[22]. Close examination indicated that obvious growth steps emerged both on the top and side surfaces. Moreover, in Figs. 1(c) and (d), due to the faster growth rate of the top surface than the side ones, evident bulge of the crystal appeared on the top surface.

More details of the chamfered edges and corners were shown in Figs. 1(b−d), where the growth steps could be distinguished clearly. The terrace growing on the base of hexagonal plate or tetragonal plate was composed of a series of smaller platelets with a displacement between adjacent two layers. The step boundaries partially became parallel with each other in the *a*-axis and *c*-axis, respectively. The area between the crossing terraces would degrade as a small facet. Furthermore, the experimental results illustrated that the particles with obvious growth steps frequently tended to have a large size. The TiB_2 in Al−5Cu matrix exhibited hexagonal or tetragonal prism with terraced structure on both the top and side surfaces consisted of a series of layered plates. A close examination indicated that the terraces were generated by two-dimensional nucleation rather than screw dislocation growth because of the lack of the screw trace on the topmost surface. Obviously, as shown in Fig. 1, on the terraced structure, the edges of the hexagonal or tetragonal planes were not affiliated to the spiral curve, but separated with similar boundaries. Moreover, it was found that on the particle surface there were multiple defects, such as scallops and the inadequacy growth of the two-dimensional nucleation, similar to the roughing transition. Actually, the roughing transition has been observed for some ceramic particles, such as NbC [23,24], TaC [25], MgO [26] and Al_2O_3 [27]. These defect points would be the effective heterogeneous nucleation points attributed to the higher free energy. Meanwhile, several fine primary crystal nucleus were observed on the TiB_2 surface.

The particle size distribution (PSD) and the particle aspect ratio distribution (PAD, the ratio of the particle diameter to thickness) were illustrated in Fig. 2. The statistic results in Fig. 2(a) manifested the PSD of TiB_2 in Al−5Cu matrix scattered in the

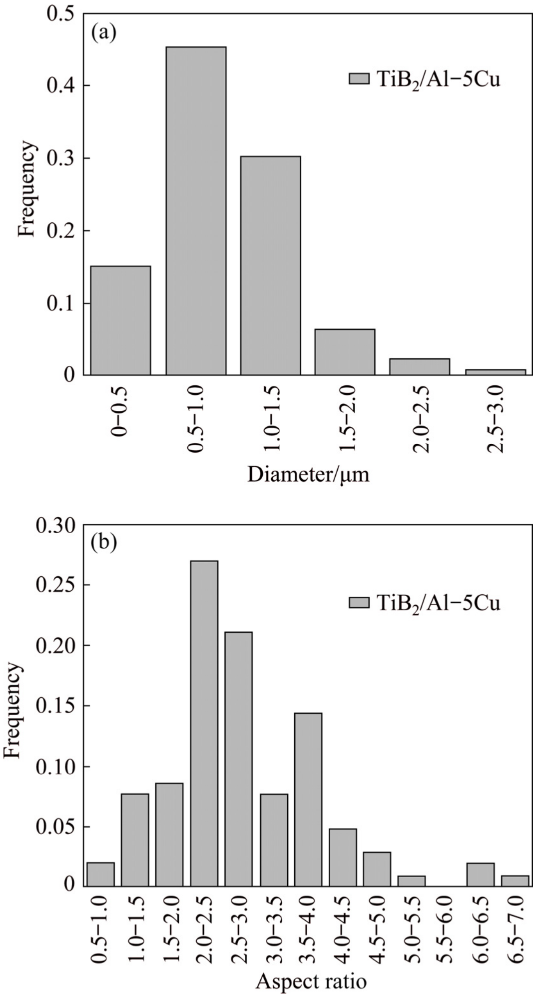

Fig. 2 Diameter distribution of TiB_2 particles in Al−5Cu matrix (a) and aspect ratio (diameter to thickness) distribution in Al−5Cu matrix (b)

range of 0−3 μm, basically conforming to the Gaussian distribution and the average TiB_2 diameter was about 0.93 μm. Compared with the PSD in monotonous Al matrix [22], the TiB_2 crystals grew up dramatically and consequently the aggregation of particles was improved notably. The PAD results were shown in Fig. 2(b). It indicated that the TiB_2 PAD accorded to the Gaussian distribution, falling in the range of 0.5−7.0. Further observation showed that some PAD distributed in the range of 0.5−1.0, indicating the rod-like TiB_2 particles in Al−5Cu. The average PAD was about 2.80, much less than that in pure Al matrix which was 3.50 in average. In conclusion, under the influence of Cu element, the TiB_2 particle size increased distinctly, especially along the *c*-axis. Hence, the aspect ratio decreased dramatically, indicating that there were more thicker particles.

In Fig. 3, obvious terraced structure appeared on the particle surface along the *a*-, *b*- and *c*-axis, respectively. The smooth flat surface lack of spiral traces implied the two-dimension nucleation mechanism. By comparison, the growth steps along the *c*-axis, marked as A, were obviously thicker than that in the *a*-axis, labeled as B, which illustrated that for TiB_2 particles both the two-dimensional nucleation and growth were more inclined to form on the basic plane than those on the side plane. Therefore, the length of A was significantly larger than that of B as shown in Fig. 3(a). Figure 3(b) showed that the multiple TiB_2 particles grew synergistically, exhibiting flower-like morphology. Detailed examination demonstrated that all the petals deposited in the same pre-platelet and on the pre-platelet surface, indeed, terraced morphology existed, verifying the aforementioned nucleation and growth difference in the two directions.

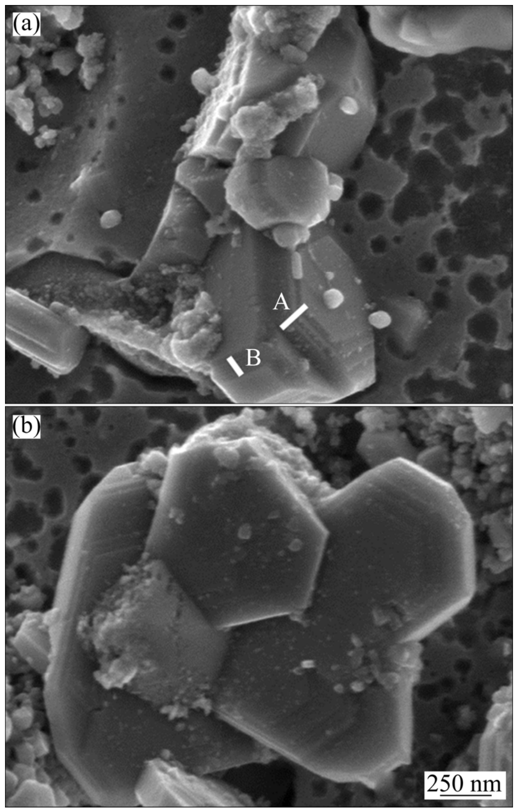

Fig. 3 Terraced morphologies of TiB_2 in Al−5Cu matrix: (a) Growth step on *c*-axis; (b) Flower-like morphology of TiB_2

Figure 4 provided clear information about the typical morphologies at different growth stages of TiB_2 in Al−Cu system. At the early stage, the TiB_2

grain exhibited spherical morphology with the size of about less than 100 nm. Afterwards, combining the energy minimization principle and the facet growth mechanism, small flat planes appeared on the curved surface. With the growth proceeding, the flat planes enlarged immediately, transforming the TiB_2 crystals into irregular polyhedrons, as illustrated in Fig. 4(c). Subsequently, the expansion of the low-index lattice planes was implemented immediately until the TiB_2 particles were exposed by (0001) and $(10\bar{1}0)$ planes for the hexagonal morphology or (0001) and $(11\bar{2}0)$ planes for the tetragonal morphology, as shown in Figs. 4(g) and (h), respectively. So far, the hexagonal or tetragonal flaky pre-platelets were achieved.

Because of the Cu element effect, as the particle evolved, the two-dimensional nucleus would generate on the defect point on the particle surface. By the repeating of the two-dimensional nucleation and the growth, the terraced morphology both on the basic surface and the side surface formed, as illustrated in Figs. 4(h, i, j). Obviously, the size of TiB_2 particles with terraced morphology increased generally, because the growth steps were on the basis of the pre-platelets.

Figure 5 schematically illustrated the growth mode of TiB_2 crystal in Al−5Cu matrix. The hexagonal particles with obvious terraced morphology grew up according to mode (I) and the flowerlike particle followed the mode (II). At the initial stage, the supersaturated degree of Ti and B elements is high in the alloy melt. Under the high temperature, the mass transport was activated with low reaction latent enthalpy between Ti and B. Therefore, it was considered that the interface between TiB_2 crystal and the melt was rough and there was no crucial nucleation barrier. New TiB_2 nuclei could be generated favorably and

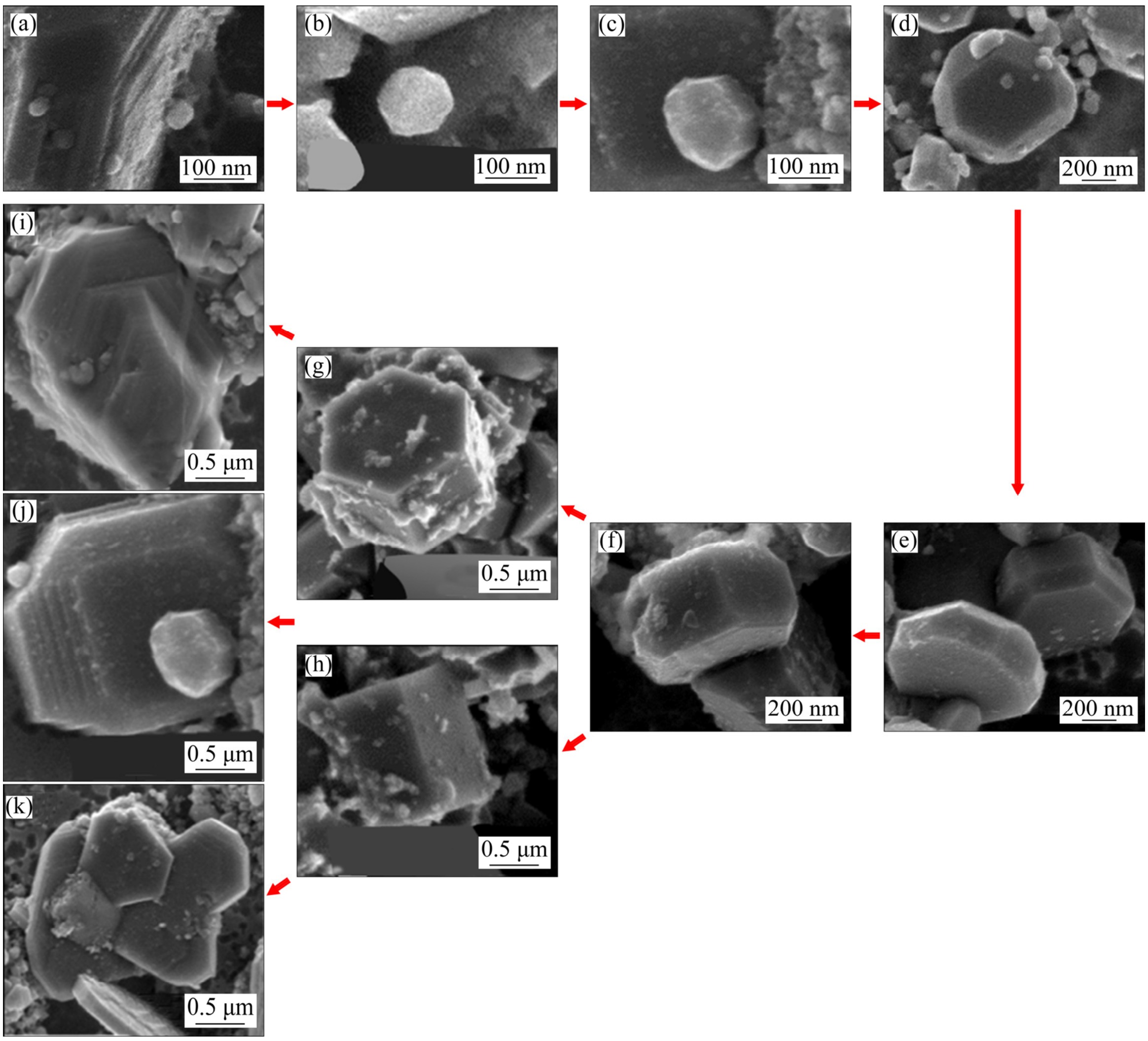

Fig. 4 Typical morphologies of TiB_2 crystal at different stages in Al−5Cu system

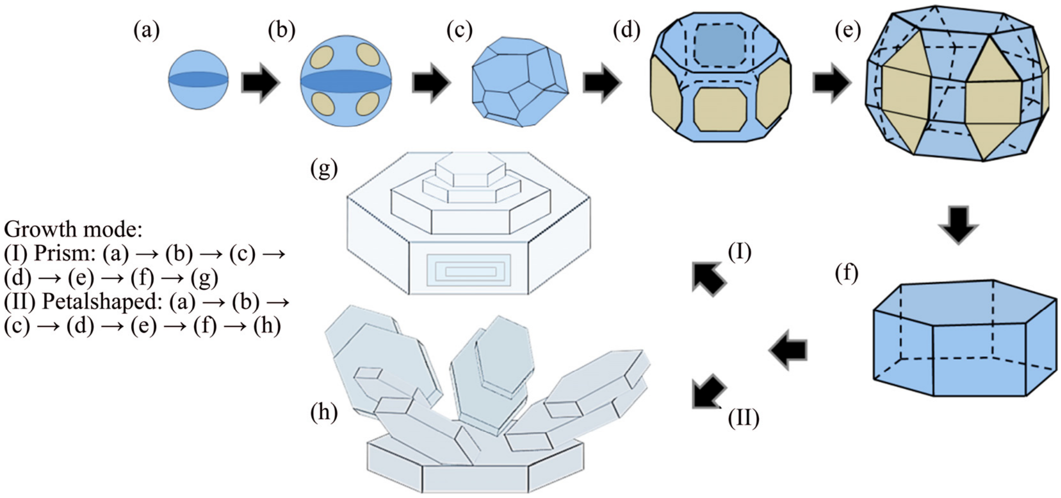

Fig. 5 Schematic representation of morphology evolution of TiB_2 in Al−5Cu matrix

subsequently experienced an isotropy growth in all directions, which would lead to the spherical or quasi-spherical grain morphology by the diffusion-controlled continuous growth. Additionally, the spherical or quasi-spherical morphology would minimize the surface energy of the composite system, as schematically shown in Fig. 5(a).

Initially, the growth of TiB_2 grains was determined by the element diffusion process. As the crystal grew, the degradation of the element supersaturation would disequilibrate the growth of the quasi-spherical TiB_2 particles. Furthermore, for TiB_2 crystals, as the atom configuration is different in various lattice planes, the surface energy is not isotropic but anisotropic. As the grains grew up, the minimization of the total surface energy could not be fulfilled by simply maintaining the spherical morphology. The final equilibrium morphology of TiB_2 was hexagonal platelet bounded with the close-packed crystal planes (0001) and the near close-packed lattice planes $(11\bar{1}0)$ rather than spherical shape, which was stimulated by a faceted growth mode [28−30]. According to the facet growth principle, some facets with the special directions would emerge on the TiB_2 spherical surface to transform towards the polyhedron morphology as shown in Fig. 5(b). As the growth proceeded, the curved surface was replaced by the facets gradually, transforming to irregular polyhedron, as illustrated in Fig. 5(c). It revealed the faceting process during the particle growth. As the TiB_2 grew, the low-index lattice planes enlarged and simultaneously, the high-index planes shrank. Successively, the incremental iteration between the low-index plane and the high-index plane was conducted uninterruptedly, and ultimately, the hexagonal TiB_2 packaged by close-packed and nearly close-packed atom arrangement formed. With the further development, the two-dimensional heterogeneous nuclei would be located on the basic (0001) surface and the $(10\bar{1}0)$ planes, generating terraced morphology. Sometimes, several nucleuses merged simultaneously in the same pre-platelet, finally forming the flowerlike morphology, as shown in Fig. 5(h).

As stated above, the TiB_2 particles in Al−5Cu exhibited small PAD, meaning the thicker crystals than those in the monotonous Al matrix. To qualitatively interpret the mentioned phenomenon, the adsorption energy ($\Delta E_{ads/surf}$) of Cu on different lattice planes of TiB_2 was calculated [31].

According to the calculation results listed in Table 1, Cu element was preferentially adsorbed in the $(10\bar{1}1)_{TiB_2}$ crystal planes, secondly the $(10\bar{1}0)_{TiB_2}$, $(11\bar{2}0)_{TiB_2}$ and $(1\bar{2}1\bar{2})_{TiB_2}$ planes and ultimately the close-packed $(0001)_{TiB_2}$ planes to maitain the minimum systematic energy. Namely, the existance of Cu element accelarated the growth of (0001) TiB_2 planes extremely, which was coincident with the abovementioned morphology characterization results.

Table 1 $\Delta E_{ads/surf}$ of Cu on different surfaces of TiB_2 (eV)

$(0001)_{TiB_2}$	$(10\bar{1}0)_{TiB_2}$	$(10\bar{1}1)_{TiB_2}$	$(11\bar{2}0)_{TiB_2}$	$(1\bar{2}1\bar{2})_{TiB_2}$
−0.0287	−0.0378	−0.0401	−0.0357	−0.0352

Generally, both the intrinsic crystallography characteristic and the external growth conditions decided the TiB_2 morphology. As the equilibrium shape, the intrinsic lattice structure prompted TiB_2 to develop into hexagonal platelet to maintain the minimum surface energy. Nevertheless, different external growth conditions usually propelled crystals to deviate from the established equilibrium growth path and transformed into various morphologies. The final crystal morphology was predicated on the balance and contradictions of the mentioned two factors.

According to the minimum energy principle, the crystal planes with higher bonding energy grew even faster to minimize the total systematic energy. As the crystal develops, these planes would shrink gradually or disappear instead. In consequence, the lattice faces with lower energy would reserve as the crystal surface at last. Namely, the TiB_2 developed into hexagonal plates with the closely packed (1000) and secondarily closely packed $(10\bar{1}0)$ exposed in the equilibrium condition. TiB_2 severely conformed to the two-dimensional nucleation and flat growth mechanism. Due to the existence of numerous alloy elements, the growth of in-situ TiB_2 in the aluminum alloy matrix was more complex to control. Under the influence of Cu, Cu was preferentially adsorbed on the $(10\bar{1}1)_{TiB_2}$ crystal plane to maintain the stability of the chamfered surface. Finally, the TiB_2 exhibited chamfered hexagonal morphology with obvious growth steps. Moreover, the growth step determined by the preferential adsorption in the *c*-axis was more prominent than that in the *a*-axis.

4 Conclusions

(1) The morphology of TiB_2 particles in three-dimensional space was examined using scanning electric microscope. Under the influence of Cu element, TiB_2 particles transformed from hexagonal plates with sharp corners and edges to chamfered hexgonal morphology with obvious growth steps and small PAD (the ratio of the particle diameter to thickness).

(2) In Al−Cu matrix, TiB_2 growth conformed to the mode: nano-scaled spherical or quasi-spherical nuclei—small facets emerging on the sphere surface—polyhedron grains—chamfered hexagonal particles—hexagonal plates—chamfered particles with obvious growth steps or flower-like morphology.

(3) Cu performed a strong adsorption on the surface of TiB_2 particles and Cu element was preferentially adsorbed in the $(10\bar{1}1)_{TiB_2}$ crystal planes, secondly the $(10\bar{1}0)_{TiB_2}$, $(11\bar{2}0)_{TiB_2}$ and $(1\bar{2}1\bar{2})_{TiB_2}$ planes, which would inhabit the growth of these faces effectively and retain a lower-energy state of the chamfered TiB_2 particles in Al−Cu matrix.

References

[1] YANG Hua-bing, GAO Tong, WU Yu-ying, ZHANG Hua-ning, NIE Jin-feng, LIU Xiang-fa. Microstructure and mechanical properties at both room and high temperature of in-situ TiC reinforced Al−4.5Cu matrix nanocomposite [J]. Journal of Alloys and Compounds, 2018, 767: 606−616.

[2] JAMIAN S, WATANABE Y, SATO H. Formation of compositional gradient in Al/SiC FGMs fabricated under huge centrifugal forces using solid-particle and mixed-powder methods [J]. Ceramics International, 2018, 45(7): 9444−9453.

[3] WU Chong-chong, GAO Tong, SUN Qian-qian, LIU Gui-liang, DU Xiao-fan, LIU Xiang-fa. A novel method of coating ex-situ SiC particles with in-situ SiC interlayer in Al−Si−C alloy [J]. Journal of Alloys and Compounds, 2018, 754: 39−47.

[4] XU Yi, LIANG Wen-ping, MIAO Qiang, WANG Ling, REN Bei-lei, CUI Shi-yu, XIA Jin-jiao, YAO Zheng-jun. Enhanced high temperature corrosion resistance of Al_2O_3/Al composite coating on γ-TiAl alloy [J]. Rare Metal Materials and Engineering, 2018, 47(4): 1075−1081.

[5] KUWABARA M, SPENCE J C H, RUHLE M. On the atomic structure of the Nb/Al_2O_3 interface and the growth of Al_2O_3 particles [J]. Journal of Materials Research, 1989, 4(4): 972−977.

[6] BISWAS P, BISWAS A, BHANDARI R, MONDAL M K. Microstructure, mechanical properties and fracture behavior of in-situ Al−5Mg−Al_4Sr composites [J]. Materials Today Communications, 2018, 15: 190−198.

[7] CHEN Gang, JIN Yu, ZHANG Hong-ming, HAN Fei, CHEN Qiang, XU Jun-rui, ZHAO Zu-de. Microstructures and mechanical properties of in-situ Al_3Ti/2024Al composites after solution and subsequent aging treatment [J]. Materials Science and Engineering A, 2018, 724: 181−188.

[8] LI Zhi-ming, CHEN Dong, WANG Hao-wei, LAVERNIA E J, SHAN A. Nano-TiB_2 reinforced ultrafine-grained pure Al produced by flux-assisted synthesis and asymmetrical rolling [J]. Journal of Materials Research, 2014, 29(21): 2514−2524.

[9] YAO X, MCDONALD S D, DAHLE A K, DAVIDSON C J, STJOHN D H. Modeling of grain refinement: Part II. Effect

of nucleant particles—TiB_2 additions for aluminum [J]. Journal of Materials Research, 2008, 23(5): 1292−1300.

[10] LIU K, NABAWY A M, CHEN X G. Influence of TiB_2 nanoparticles on elevated-temperature properties of Al−Mn−Mg 3004 alloy [J]. Transactions of Nonferrous Metals Society of China, 2017, 27(4): 771−778.

[11] WU Ning, XUE Feng-dan, YANG Hai-lin, LI Guo-ping, LUO Feng-hua, RUAN Jian-ming. Effects of TiB_2 particle size on the microstructure and mechanical properties of TiB_2-based composites [J]. Ceramics International, 2019, 45(1): 1370−1378.

[12] ZHANG Ting-ting, FENG Kai, LI Zhu-guo, KOKAWA H. Effects of in-situ synthesized TiB_2 on crystallographic orientation, grain size and nanohardness of AA6061 alloy by laser surface alloying [J]. Materials Letters, 2019, 253: 213−217.

[13] QI Li-qiang, HAN Tian-yi, ZHANG Ya-juan. Electrostatic precipitability of TiB_2−Fe−Mo−Co ceramic-metal composites [J]. Journal of Alloys and Compounds, 2019, 778: 507−513.

[14] XIA Meng, FENG Yi, TIAN Pei, SONG Zhao-kun, ZHAO Lan, CAI Cheng-yu. Quantitative analysis of TiB_2 particles and properties of Cu−TiB_2 composite prepared by in situ reaction [J]. Rare Metal Materials and Engineering, 2017, 46(11): 3260−3266.

[15] ZOU Cun-lei, KANG Hui-jun, WANG Wei, CHEN Zong-ning, LI Ren-geng, GAO Xiao-xia, LI Ting-ju, WANG Tong-min. Effect of La addition on the particle characteristics, mechanical and electrical properties of in situ Cu−TiB_2 composites [J]. Journal of Alloys and Compounds, 2016, 687: 312−319.

[16] SHARMA R, SINGH A K, ARORA A, PATI S, DE P S. Effect of friction stir processing on corrosion of Al−TiB_2 based composite in 3.5 wt.% sodium chloride solution [J]. Transactions of Nonferrous Metals Society of China, 2019, 29(7): 1383−1392.

[17] THADELA S, MANDAL B, DAS P, ROY H, LOHAR A K, SAMANTA S K. Rheological behavior of semi-solid TiB_2 reinforced Al composite [J]. Transactions of Nonferrous Metals Society of China, 2015, 25(9): 2827−2832.

[18] NIE Jin-feng, WANG Fang, LI Yu-sheng, LIU Yan-fang, LIU Xiang-fa, ZHAO Yong-hao. Microstructure and mechanical properties of Al−TiB_2/TiC in situ composites improved via hot rolling [J]. Transactions of Nonferrous Metals Society of China, 2017, 27(12): 2548−2554.

[19] CHEN Fei, WANG Tong-min, CHEN Zong-ning, MAO Feng, HAN Qiang, CAO Zhi-qiang. Microstructure, mechanical properties and wear behaviour of Zn−Al−Cu−TiB_2 in situ composites [J]. Transactions of Nonferrous Metals Society of China, 2015, 25(1): 103−111.

[20] GAO Xiang-dong, LI Xiao-min, GAO Wei, QIU Ji-jun, GAN Xiao-yan, WANG Cai-lu, LENG Xue. Nanocrystalline/nanoporous ZnO spheres, hexapods and disks transformed from zinc fluorohydroxide, their self-assembly and patterned growth [J]. Cryst Eng Comm, 2011, 13(14): 4741−4747.

[21] BISWAS S, SUNDSTROM V, DE S. Facile synthesis of luminescent TiO_2 nanorods using an anionic surfactant: Their photosensitization and photocatalytic efficiency [J]. Materials Chemistry and Physics, 2014, 147(3): 761−771.

[22] SUN Jing, ZHANG Xiao-bo, ZHANG Yi-jie, MA Nai-heng, WANG Hao-wei. Effect of alloy elements on the morphology transformation of TiB_2 particles in Al matrix [J]. Micron, 2015, 70: 21−25.

[23] JAYAPRAKASH C, SAAM W F, TEITEL S. Roughening and facet formation in crystals [J]. Physical Review Letters, 1983, 50(25): 2017−2020.

[24] WARREN R. Microstructural development during the liquid-phase sintering of two-phase alloys, with special reference to the NbC/Co system [J]. Journal of Materials Science, 1968, 3(5): 471−485.

[25] MOON H, KIM B L, KANG S J. Growth mechanism of round-edged NbC grains in Co liquid [J]. Acta Materialia, 2001, 49(7): 1293−1299.

[26] YOON D Y, CHO Y K. Roughening transition of grain boundaries in metals and oxides [J]. Journal of Materials Science, 2005, 40(4): 861−870.

[27] VLACH K C, SALAS O, NI H, JAYARAM V, LEVI C G, MEHRABIAN R. A thermogravimetric study of the oxidative growth of Al_2O_3/Al alloy composites [J]. Journal of Materials Research, 1991, 6(9): 1982−1995.

[28] CHEN G Y, LAN C W. On the growth orientation of twin-related faceted dendrites [J]. Scripta Materialia, 2016, 125: 54−57.

[29] ANGUS J C, SUNKARA M, SAHAIDA S R, GLASS J T. Twinning and faceting in early stages of diamond growth by chemical vapor deposition [J]. Journal of Materials Research, 1992, 7(11): 3001−3009.

[30] KANG Hui-jun, WANG Tong-min, LI Xin-zhong, SU Yan-qing, GUO Jing-jie, FU Heng-zhi. Faceted–nonfaceted growth transition and 3-D morphological evolution of primary Al_6Mn microcrystals in directionally solidified Al−3 at.% Mn alloy [J]. Journal of Materials Research, 2014, 29(11): 1256−1263.

[31] CHEN Lei, WANG Hui-yuan, LI Yan-jun, ZHA Min, JIANG Qi-chuan. Morphology and size control of octahedral and cubic primary Mg_2Si in an Mg−Si system by regulating Sr contents [J]. Cryst Eng Comm, 2014, 16(3): 448−454.

Cu 元素对 TiB_2/Al−Cu 复合材料中 TiB_2 形貌的影响

孙 靖[1,2]，王旭琴[1]，陈 艳[1]，王 飞[1]，王浩伟[2]

1. 上海航天设备制造总厂有限公司，上海 200245；
2. 上海交通大学 金属基复合材料国家重点实验室，上海 200240

摘 要：为了探究 Cu 元素对原位自生 TiB_2 颗粒形貌演变的影响，通过混合盐铸造技术制备 10%(质量分数)TiB_2 增强 Al−5%Cu(质量分数)复合材料。采用多尺度显微组织表征及统计方法研究 Cu 元素引起的 TiB_2 增强相的形貌表征及演变。在控制铸造下，当添加质量分数为 5%的 Cu 元素时，TiB_2 形貌颗粒由具有尖角的六方片状演变成具有倒角的六方或四方棱柱状，同时在颗粒表面和侧面均存在明显的生长台阶。TiB_2 颗粒在 Al−Cu 基体中生长遵循以下规律：纳米尺度的球形晶核—多面体晶核—具有倒棱角的六方棱柱—六方片状—具有明显生长台阶的颗粒。通过计算 Cu 在 TiB_2 不同晶面上的吸附能揭示其影响机理，计算结果表明 Cu 优先吸附在$(1011)_{TiB_2}$晶面上，促使最终生成的 TiB_2 具有较小的径厚比。

关键词：形貌控制；优先吸附；TiB_2 形貌；二维形核；生长台阶

(Edited by Xiang-qun LI)